CFD Letters www.cfdl.issres.net Vol. 2(1) – March 2010

Numerical simulation and CFD-Based Correlation of Erosion Threshold Gas Velocity in Pipe Bends

Samy M. El-Behery[1c], Mofreh H. Hamed[2], M. A. El-Kadi[1] and K. A. Ibrahim[1]
[1] *Mechanical Power Engineering Department, Faculty of Engineering, Minoufiya University, Shebin El-kom, EGYPT*
[2] *Mechanical Engineering Department, Faculty of Engineering, Kafrelsheikh University, Kafrelsheikh, EGYPT*

Received: 12/08/2009 – Revised 04/01/2010 – Accepted 18/02/2010

Abstract

This paper presents numerical simulation of sand erosion phenomena in curved ducts. The Eulerian-Lagrangian approach is used to simulate the gas-solid two-phase flow while semi-empirical model is used to calculate the erosion rate. The effect of solid phase on the gas phase is included in the model. The model prediction is validated with the available experimental data and good agreement was obtained. Based on many predictions of the maximum penetration rate, a CFD based correlation is developed to calculate the penetration rate in bends. From this equation a model to predict the erosional velocity was developed. The present results showed that the flow velocity should be decreased as the mass loading ratio, particle size, pipe diameter increase in order to avoid failure.

Keywords: Gas-solid, Erosion, Bend, Numerical simulation, Two-phase

1. Introduction

Erosion is a complex process that is affected by numerous factors and small or subtle changes in operational conditions can significantly affect the damage it causes. This can lead to the scenario in which high erosion rates occur in one production system, but very little erosion occurs in other seemingly very similar systems [1]. Metal loss was primarily due to mechanical forces which are induced by solid particles, liquid droplet, or cavitation.

The current oil and gas industries practice for sizing process piping, flow lines, pipelines and tubing limits the flow velocity to the maximum erosional velocity, V_e as calculated by American Petroleum Institute Recommended Practice 14E (API RP 14E) equation [2]:

$$V_e = \frac{C}{\sqrt{\rho_m}} \tag{1}$$

For solids-free fluids values of constant, C are 100 and 125 for continues service and intermittent service, respectively, are conservative. The recommended practice adds: "If solids production is anticipated, fluid velocity should be significantly reduced. Different values of constant, C may be used where specific application studies have shown them to be appropriate."

It is obvious that Eq. (1) is very simple and easy to use, but the equation does not account for many factors contributing to erosion such as particle size and density, mass loading ratio and

---

[c] Corresponding Author: Samy M. El-Behery
Email: s_elbehery@yahoo.com Telephone: + 20102292318 Fax: +20482235695.

type of geometry. The only physical variable accounted for in Eq. (1) is the fluid density. The equation suggests that the limiting velocity could be higher when the fluid density is lower. This does not agree with experimental observation for sand erosion, because sand in gases with lower densities will cause higher erosion rates than liquids with higher densities [2-8]. Therefore, the form of Eq. (1) does not seem to be appropriate for situation involving sand production.

Recognizing the limitations of API RP 14E in the presence of sand, several investigators have developed models for erosion prediction or erosional velocities. Most of these models are for erosion in bends, since bends are especially susceptible to erosion. Many of these models are based on an impact damage model of the form:

$$ER = AW_{p1}^{n}F(\alpha_1) \tag{2}$$

where, ER is the erosion rate (kg of material removed/kg of sand hitting it). W_{p1} is the particle impact velocity on the metal surfaces. This velocity depends on the flow condition, the geometry of the component and sand properties. A and n are experimentally determined constant depending on the material being eroded and other factors. α_1 is the particle impact angle and $F(\alpha_1)$ is a material dependent function of the impact angle between 0 and 1. Furthermore, the Tulsa model [5, 7] relies on empirical formula to account for particle tracking while the Huser and Kvernvold [8] model allows actual calculation and the values of A, n and $F(\alpha_1)$ are derived from sand-blasting tests on small material samples [9].

The main objective of the work presented herein is to adopt a numerical procedure to predict sand erosion phenomena in curved duct. Then the data generated from numerical prediction is to be used to develop a CFD based correlation that can be used to calculate the erosional velocity in pipe contains bends.

2. Mathematical model

The Euler-Lagrange approach was applied in the calculation of gas-solid flow in bends by solving the Reynolds-averaged Navier-Stokes (RANS) equations together with a turbulence model. The previous study by the present authors [10] showed that the RNG based k-ε turbulence model of [11] predicts the flow within the bend better than the standard k-ε model, low Re k-ε model of [12] and the extended k-ε model of [13]. Therefore, the RNG based k-ε is recommended in the present study. Movements of particles are simulated by accounting for all the important forces. The coupling effect of solid particles on the gas phase is described through modifications of gas phase equations. This is achieved by introducing the void fraction which is defined as the volume of a phase divided by the volume of the two phases, and momentum exchange source term in the gas phase equations. The gas phase is considered as a continuous phase, and the solid phase is accounted for as a dispersed phase. Some simplifying assumptions are made to provide a reasonable solution for engineering objectives.

2.1. Model Assumptions

1. The flow model is for a two-dimensional bend therefore, the influence of span-wise velocity on the particle motion is not included.
2. The particles are spherical in the particle tracking procedure. However, the erosion ratio model in the present study is based on the experimental data for sand particles (the erosion ratio is defined as the ratio of mass loss of the target material by the mass of particles impinging on the target material).
3. The effect of inter-particle collisions is ignored since inertial effects prevail.
4. The effects of turbulent flow velocity fluctuations on the particles are not considered. This assumption reduces the applicability of the model to geometries that redirect the flow such as elbows. There situations, however, where the effects of turbulent fluctuations on the particle motion can not be ignored such as flow with particles in a straight pipes [6].

5. The ratio between particle density and gas density is very high so the effects of added mass force, pressure gradient force on the particle are neglected in the present study.

2.2. Gas Flow Modeling

The general form of elliptic differential equations governing two-dimensional, turbulent, steady, incompressible and isothermal two-phase flow through curved duct with upstream and downstream straight ducts is given by

$$\frac{1}{y^j}\frac{\partial}{\partial y}\left(\alpha\rho y^j v\Phi\right)+\frac{1}{y^j}\frac{\partial}{\partial\theta}\left(\alpha\rho u\Phi\right)=\frac{1}{y^j}\frac{\partial}{\partial y}\left(\alpha\Gamma_\Phi y^j\frac{\partial\Phi}{\partial y}\right)+\frac{1}{y^j}\frac{\partial}{\partial\theta}\left(\alpha\Gamma_\Phi\frac{\partial\Phi}{y^j\partial y}\right)+S_\Phi-S_S^\Phi+\rho g^\Phi \tag{3}$$

where, $j = 1$, $y = r$ for curved duct, while for straight ducts $j = 0$, $\theta = x$. and the S^Φ and S_S^Φ are source terms of gas and dispersed phases respectively. Constants of the used turbulence model are are taken as in [11].

The effective and eddy viscosities are taken and calculated as in [11],

$$\mu_{eff}=\mu\left[1+\sqrt{\frac{C_\mu\rho}{\mu}\frac{k}{\sqrt{\varepsilon}}}\right]^2 \quad , \mu_t=\mu_{eff}-\mu \tag{4}$$

The effect of particulate phase on the turbulent structure can be written as reported in [11] for k and ε equations, respectively, as follows,

$$S_S^k=2k\left[\frac{\rho_p}{\tau_p}\right]\left[1-\exp(-\mathrm{B}_k\frac{\tau_p}{\tau_l})\right] \tag{5}$$

$$S_S^\varepsilon=2\varepsilon\left[\frac{\rho_p}{\tau_p}\right]\left[1-\exp(-\mathrm{B}_\varepsilon\frac{\tau_p}{\tau_l})\right] \tag{6}$$

2.3. Particulate Phase Modeling

The solid phase is simulated using the Lagrangian approach. A few thousands of computational particles ((i.e. parcels)) were traced through the flowfield for each coupled iteration. After each given time step the new position of the parcels and the new transitional and angular velocities are calculated from the equations of motion as in [14] through,

$$\frac{d\vec{X}_p}{dt}=\vec{U}_p \tag{7}$$

$$m_p\frac{d\vec{U}_p}{dt}=\vec{F}_D+\vec{F}_{LS}\;\vec{F}_{LR}\;+\vec{F}_g \tag{8}$$

$$I_p\frac{d\vec{\omega}_p}{dt}=\vec{T} \tag{9}$$

$$\vec{T}=\pi\mu D_p^3\left\lfloor 0.5\nabla\times\vec{U}-\vec{\omega}_p\right\rfloor \tag{10}$$

where, $\vec{X}_p$ is the particle position vector, $\vec{U},\vec{U}_p$ are the gas and particle velocity vectors, $\vec{\omega}_p$ is the particle angular velocity vector, T is the torque acting on the particle, $I_p = 0.1 m_p D_p^2$ is the particle moment of inertia and m_p is the particle mass, $\vec{F}_D$, $\overrightarrow{F_{LS}}$, $\vec{F}_{LR}$ ***and*** $\vec{F}_g$ are the components of the force arising from drag, shear lift, Magnus lift due to particle rotation and gravity, respectively. Detailed description of these forces can be found in [10]

For the calculation of particle motion, the equations of particle motion are integrated using fourth order Runge Kutta method. To achieve this, the local values for the linear and angular velocities components, the liquid viscosity, turbulent kinetic energy and its dissipation rate at the location of the particle are required. These local values at the particle center are linearly interpolated from values at the closest grid nodes of the fluid finite-difference scheme enclosing the particle.

2.4. Coupling between the Two Phases

The particles occupy the computational cell and reduce the gas volume fraction. They also exert interaction forces on the surrounding gas phase. Thus, the two phases are coupled through the gas volume fraction and through the total source term, S_s^{Φ} that accounts for the momentum exchange between solid particles and the gas phase (two-way coupling).

The void fraction for dispersed phase, β and for gas phase, α are calculated using trajectory method, as given in [18] as,

$$\beta = \sum_{traj} \frac{n_k \Delta t_k V_p}{V_C} \quad , \quad \alpha = 1 - \beta \tag{11}$$

here, n_k is the number of actual particles in the computational particle (parcel) *k*, V_P is the volume of the particle, V_c is the volume of computational cell and $\sum_{traj}$ means summing over all trajectories passing through the computational cell. It was assumed that each parcel contains several particles with the same properties and the number of actual particles in each parcel is obtained by dividing the total number of flowing particles by the number of simulated parcels. The source term of dispersed phase in the gas momentum equation is calculated as in [14] by,

$$S_s^{u,v} = \frac{\beta \rho_p}{m_p n} \sum_{k=1}^{n} \left(\vec{F}_{D_k} + \vec{F}_{LR_k} + \vec{F}_{LS_k} \right) \tag{12}$$

where, n is the number of trajectories passing through the computational cell.

2.5. Erosion Model

To compute the erosion rate, *ER*, a semi empirical relation for sand erosion given by [19] is used,

$$ER = A F_s W_{p1}^{n} F(\alpha_1) \tag{13}$$

where, $F(\alpha_1)$ is a function depends on impact angle and material being eroded and is given by;

$$F(\alpha_1) = \begin{cases} a\alpha_1 + b\alpha_1 & \alpha_1 \le \alpha_o \\ \Psi \cos^2 \alpha_1 \sin(\varpi \alpha_1) + \Omega \sin^2 \alpha_1 + ƛ & \alpha_1 > \alpha_o \end{cases} \tag{14}$$

The values of the empirical constants based on W_{p1} in ft/sec are taken as in [19]. W_{p1} and α_1 are the impact velocity and impact angle, respectively, as shown in Fig. 1. The F_S coefficient accounts for sand sharpness.

If the erosion in kg/kg is multiplied by the sand flow rate the erosion rate in kg/sec will be obtained. The penetration rate is obtained by dividing the erosion rate by the local cell area and by the density of the wall material.

2.6. Boundary Conditions

At the inlet, the axial velocity profile for gas phase is assumed fully developed turbulent velocity profile, where the radial velocity is assumed to be zero. At outlet, the gradient of flow variables in the flow direction is set equal zero; $\partial \Phi / \partial x = 0.0$ (Neumann conditions), and the radial velocity v is set to zero. At the solid wall boundaries, however, $u = v = 0.0$, no-slip conditions. Because the k and ε equations are not solved at the grid point adjacent to the wall, a modeling scheme is required to simulate the variation of eddy viscosity, μ_t. For this purpose the mixing length approach is adopted where the eddy viscosity is modeled as a function of mixing length as in [20].

2.7. Particle Wall Interaction

The particle-wall collision occurs when the distance between the particle centre and the wall is less than the particle radius. The condition of rebound is achieved if the particle velocity before collision, w_{p1} is greater than the critical particle velocity, $w_{p,cr}$ as in [21]. The solution of the momentum equations with Coulombs law of friction yields a set of equations for sliding and non-sliding collision process [22].

3. Solution Procedure

A hybrid discretization scheme is used for the momentum, turbulent kinetic energy and dissipation rate equations of the gas phase while the equations of particle motion are integrated using fourth order Runge Kutta method. The mathematical model using Eulerian-Lagrangian approach as well as wall erosion sub-model was implemented in a FORTRAN program in which the equations of motion are repetitively solved for each representative particle. The boundary conditions and particle-wall interaction are also incorporated. The continuous phase flow is obtained using the SIMPLE approach described by Patankar [23]. The motion of each parcel is then followed in a Lagrangian frame using the forces generated by fluid motion and gravity. The effect of particles on the local flowfield must then be modeled and fed back into the flowfield for the next iteration of gas calculations. The procedure is repeated until the maximum error in the axial gas velocity between two successive coupled iterations is less than 0.5% of the inlet mean velocity. Fig. 2 shows the history of the axial momentum residuals. The momentum residuals fluctuate during the two-way coupling process, even though the gas phase solution converges to a prescribed tolerance (0.001) for every coupling. Residuals of radial momentum and continuity show a similar kind of fluctuations. During the calculation the impact location, angle and velocity are stored and used in the erosion sub-model after the overall convergence is achieved.

The selection of the grid size influences the obtained solution and its selection represents a compromise between the accuracy and computer time. Therefore, at the beginning of each run, the computer program performs the calculation for gas phase only for different grid sizes. The axial gas velocity at bend exit is compared for different grid sizes. If the difference in axial gas velocity at bend exit in case of fine grid and coarse grid is less than 0.5% of the mean inlet velocity, the coarse grid was chosen. Uniform grid in both directions is used, and the value of the dimensionless wall distance, y+ for the cell adjacent to the wall, is in the range of 30-60 for all simulations.

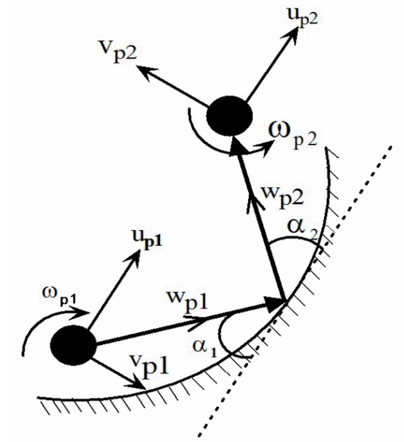

Figure 1. Definition of velocities and angles before impact and after rebound.

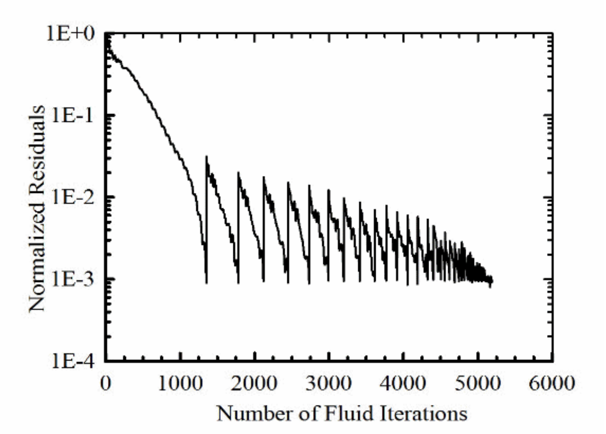

Figure 2. Convergence history for two-way coupling ($\delta = 0.33$, $U_o = 20$ m/s, $D_p = 100$ µm and $D = 0.1$ m).

4. Results and discussion

The value of time step, *Δt* and the number of computational particles are chosen to ensure independent results. To reach this condition, several simulations are performed using different time steps and deferent number of parcels for each condition. The effect of time step on the penetration rate profiles is shown in Fig. 3. It can be seen that, after a certain value of *Δt*, the results is independent of the time step. Similar results are reported in Fig. 4 for the effect of number of parcels. Based on these results, the time step is selected to be 10^{-6} sec. and the number of parcels was chosen to be 10000 parcels.

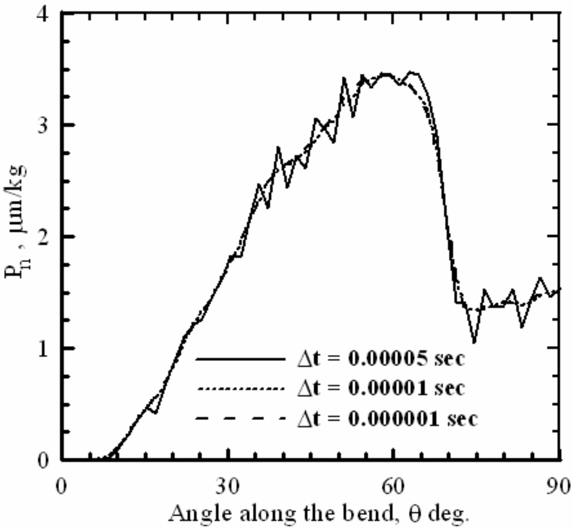

Figure 3. Effect of Lagrangian time step, *Δt* on the penetration rate profile (conditions as in Fig. 2).

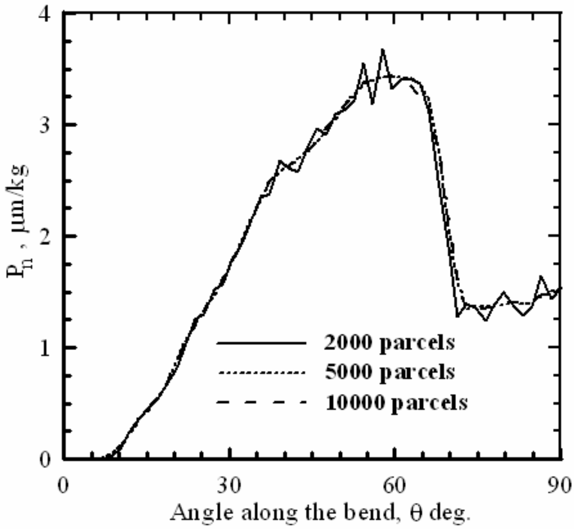

Figure 4. Effect of number of parcels on the penetration rate profile (condition as in Fig. 2).

To validate the present flow model, the predicted radial and axial velocities for both phases and the particle concentration are compared with the measured ones of [24 and 25] and presented in [10]. The comparisons with the experimental and numerical results of Wadke et al. [26] are presented in the present paper. Single particle trajectory was traced numerically and experimentally in a 90^o horizontal-to-vertical curved duct. The time required for the particle to travel from feeding point to the end of horizontal pipe and the time required for the particle to travel from the feed point to end of the bend were measured. In the present prediction the particle is released at the feed point at zero transitional and rotational velocities. The particle after that is transported under the effect of gravity and aerodynamic forces. The tested bend dimensions and flow conditions were taken as in [26]. The trajectory of such particle is shown in Fig. 5.

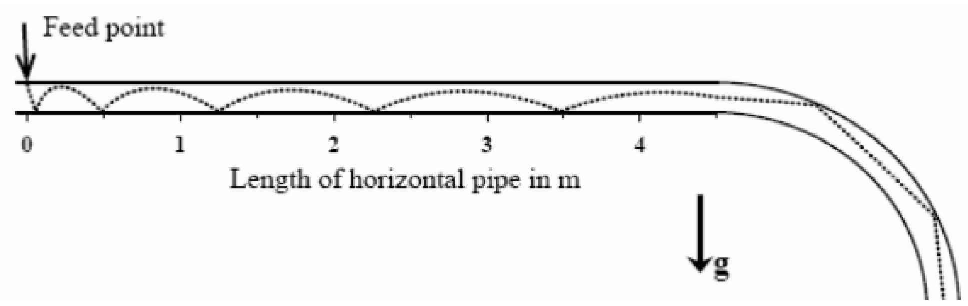

Figure 5. Particle trajectory at a velocity of 20 m/sec (the horizontal and vertical scales are not the same).

Figure 6 shows comparisons between the present predicted time (the time required for the particle to travel from feed point to the end of horizontal pipe and to the end of the bend) and the measured and predicted results of [26]. A very good agreement between the present predictions and measured data is obtained. The present model predicts the time required for the particle to travel to the end of the bend at higher values than those of [26] as shown in Fig. 6.b. This may be due to the assumption, of fully developed velocity profile at every section, given in [26].

The erosion model is validated by comparing the present predictions with experimental data reported in [4, 6-7] and with the experimental data of Bikbaev et al. [27]. Figure 7 presents a comparison between present predictions and experimental results reported in [4, 6-7]. The sand flow rate is 1.02 ft^3/day (1.2×10^{-3} m^3/hr) and the flow velocity changes from 9.15 to 30.5 m/sec. It can be seen from Fig. 7 that the model prediction agrees very well with the experimental data. Figure 8 shows comparisons between present predicted and measured penetration rates given by [27] at different mass loading ratios. It can be seen from the figure that the present model predicts the maximum penetration rate for smaller loading ratio (*Mr* =0.57) fairly well, as the mass loading ratio increase the model over-predict the maximum penetration rate. The major contribution to the discrepancy between predicted values and data of [27] may be due to the interaction between sand particles where the present model neglects this effect.

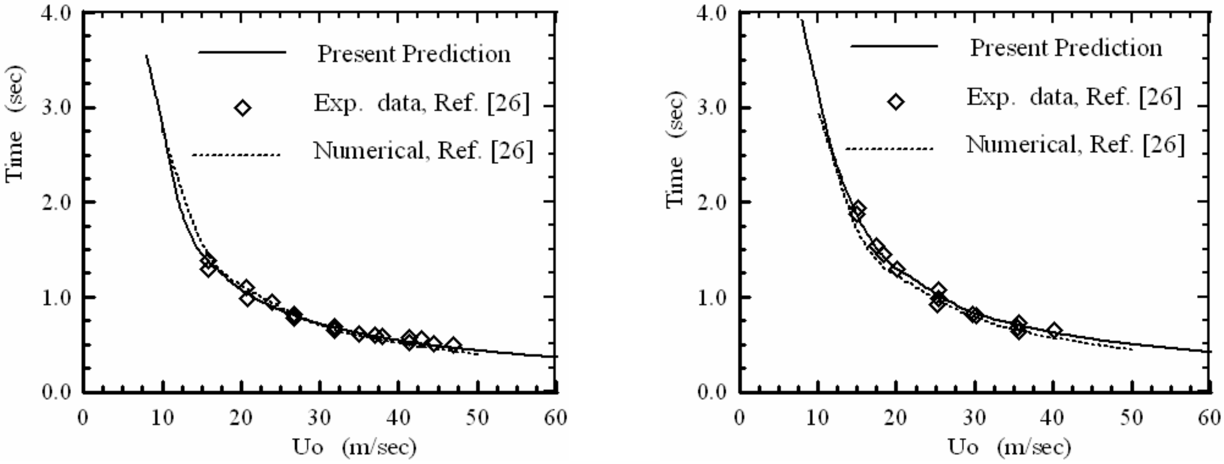

a- Time required for particle to travel from the feed point to the end of the horizontal pipe.

b- Time required for particle to travel from the feed point to the end of the bend.

Figure 6. Comparisons between predicted time and the published data of [26].

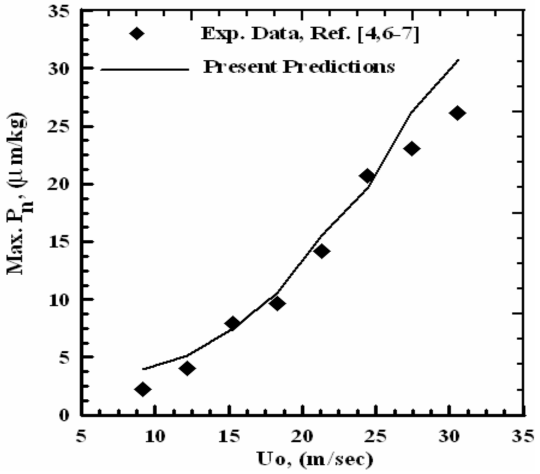

Figure 7. Comparison between predicted maximum penetration rate and Exp. data reported in [4, 6-7]

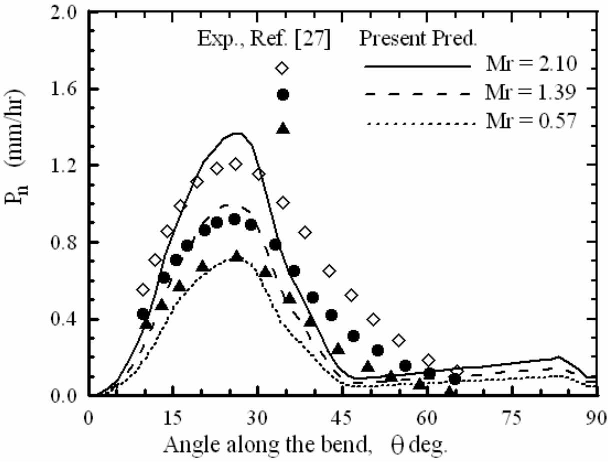

Figure 8. Comparison between the predicted penetration rate and the experimental data of [27].

In the present work, based on many CFD predictions of erosion rate and on the curve fitting of maximum penetration rate results, a new CFD based correlation is developed and is recommended as an approximate engineering calculations used for calculating the effect of different parameters on the maximum penetration rate in 90^o bends. The following correlations are recommended;

$$P_n\big|_{\max}(\mu m/kg)=\begin{cases}\dfrac{6.74\times10^{-4}F_s.BH^{-0.59}.D_p^{0.595}.U_o^{1.61}}{D^{1.7}.Mr^{0.1}.e^{0.068/\delta}} & , \quad D_p \le D_{pcr}\\[2ex] \dfrac{0.012F_s.BH^{-0.59}.U_o^{1.63}}{D^{1.66}.Mr^{0.0924}.e^{0.069/\delta}} & , \quad D_p > D_{pcr}\end{cases} \tag{15}$$

where,

$$D_{pcr}=126\frac{U_o^{0.034}.D^{0.068}.Mr^{0.013}}{e^{1.71\times10^{-3}/\delta}} \tag{16}$$

In the above correlation D_{pcr} is defined as the particle size in μm at which the penetration does not be affected by particle diameter. This behavior, from the authors' point of view, is due to that, as the particle diameter increases the particle inertia increase, which leads to an increase in the penetration rate. On the other hand, for constant mass loading ratio the number of particles within the flowfield decreases, this leads to a decrease in the penetration rate. Thus, at a certain particle diameter, D_{pcr}, depending on the flow and geometric parameters, the two effects cancel each others.

For a wide range of operating condition, the critical particle, D_{pcr} is found to vary between 100 and 200 μm. It should be noted that the above correlation is based on the condition that the sand particle density is around 2650 kg/m^3 and the carrier fluid is air at standard condition (ρ = 1.22 kg/m^3 and μ = 1.82×10^{-5} pa.s). If the particle density or fluid properties deviate significantly from above values, it is recommended that the flow modeling and particle tracking procedure be used instead of this simplified model. Furthermore, the correlation was based on simulation with particle diameter ranging from 40 to 500 μm, curvature ratio between 0.05 and 0.65, pipe diameter ranging between 0.025 and 0.4 m.

The accuracy of Eq. (15) is demonstrated by comparing its predictions with measured and predicted penetration rates in pipe bends by different investigators under different conditions. The results of this comparison are given in table 1 (see appendix). The error of the predicted penetration rates against the number of data points (as a histogram) is presented in Fig. 9. The predictions of Salama [4] were based on the following Equation:

$$P_n\big|_{\max}=\frac{1}{S_m}\frac{\overset{o}{m}_s V_m^2 D_p}{D^2\rho_m} \tag{17}$$

In the above equation S_m is a geometry dependent constant, specified by Salama [4].

Figure 9 indicates that more than 75% of the predicted penetration rate is in the error range ±50%. Although this error is high, it is quite acceptable for complex mixture and erosion prediction where a large number of uncontrolled parameters act.

To obtain the erosional velocity limits for air-solid flows at standard pressure and temperature, multiplying Eq. (15) by $\overset{o}{m}_s$ ($\overset{o}{m}_s=\frac{\pi}{4}D^2U_o\rho Mr$) and rearranging for the flow velocity in terms of penetration rate in μm/sec and operating parameters as follow:

$$V_e = \begin{cases} \left[\dfrac{1550 P_n B H^{0.59} e^{0.068/\delta}}{Mr^{0.9} F_s D^{0.3}} \right]^{0.38} & , \quad D_p \le D_{pcr} \\ \left[\dfrac{87 P_n B H^{0.59} e^{0.069/\delta}}{Mr^{0.91} F_s D_p^{0.595} D^{0.34}} \right]^{0.38} & , \quad D_p \le D_{pcr} \end{cases} \tag{18}$$

The erosional velocity model proposed by Salama [4] has the following form:

$$V_e = \left[\frac{20 P_n}{Mr D_p} \right]^{1/3} \tag{19}$$

where, P_n = Penetration rate in mm/year and a limiting value of D_p = 400 μm should be used if $D_p >$ 400 μm.

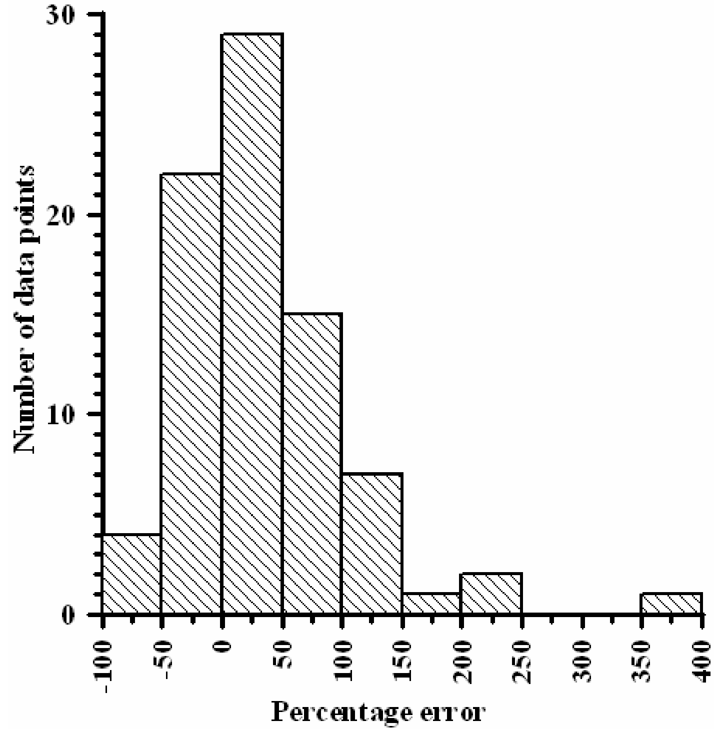

Figure 9. The error of the predicted penetration rates using the proposed correlation against the number of data points.

Figure 10 presents a comparison between the predicted erosional velocity limits by the present model, equation (18), and Salama's model, equation (19), in terms of mass loading ratio. It can be seen from the figure that both models have the same trend and the present model accounts for the effect of bend geometry. The figure shows also that the flow velocity should be decreased as the mass loading ratio increases in order to avoid failure. This is due to that, as the mass loading ratio increases the penetration rate in μm/sec increases. The present model predictions indicate that the erosional velocity increases as the curvature ratio decreases. This is due to the decrease in penetration as the curvature decreases. The figure shows also that, as the pipe diameter increases the erosional velocity decreases. This may be due to that, as the pipe diameter increases the sand flow rate increases for a certain mass loading ratio which resulting in an increase in the penetration rate.

Equations (18) and (19) can be rewritten to predict the erosional velocity limits in terms of sand flow rate, $\overset{o}{m}_s$ as follow:

$$V_e = \begin{cases} \left[\dfrac{1500P_n BH^{0.59} e^{0.068/\delta} D^{1.5}}{Mr^{0.9} F_s D_p^{0.595}}\right]^{0.58} & , \; D_p \le D_{pcr} \\ \left[\dfrac{84P_n BH^{0.59} e^{0.069/\delta} D^{1.48}}{Mr^{0.91} F_s}\right]^{0.6} & , \; D_p \le D_{pcr} \end{cases} \tag{18}$$

$$V_e = D\left[\frac{19P_n}{\overset{o}{m}_s \, D_p}\right]^{1/2} \tag{19}$$

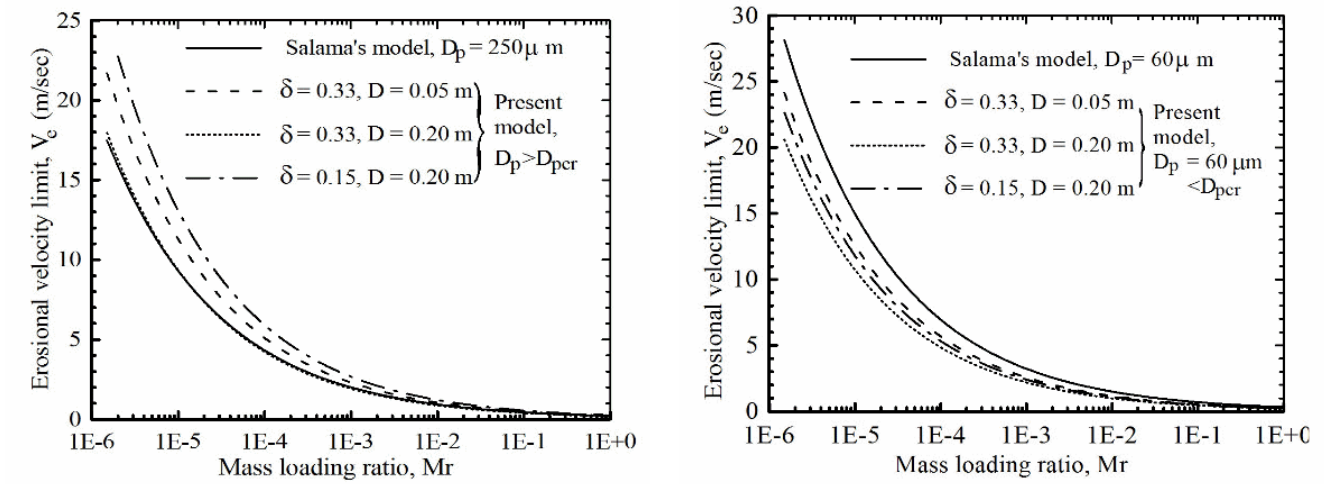

a- Large particle.

b- Small particle.

Figure 10. Effect of mass loading ratio on the erosional velocity limits, (allowable penetration rate = 0.1mm/year, *BH* = 120 and sharp particle).

Figure 11 presents a comparison between the predictions of the present model, equation (18), and that of Salama's model, equation (19), in terms of pipe diameter. It can be seen from the figure that the erosional velocity limits increases as the pipe diameter increases. This is due to that, the penetration rate decreases as the pipe diameter increases at constant sand flow rate. Furthermore, the two models are compared in terms of sand flow rate in Fig. 12. It can be seen from the figure that, as the sand flow rate increases the erosional velocity limits decreases. This is due to the increase in penetration rate as the sand flow rate increases. The figures also indicate that the mass loading ratio increases as the erosional velocity decreases. Figures 11.b and 12.b show that the predictions of Salam's model give higher values of V$_e$ than the present predictions. This may be due to that, the effects of secondary flow and turbulence dispersion on the particles motion, which are neglected in the present study. Therefore, further work including the effects of turbulence dispersion and secondary flow (3-D simulations) is needed to assess the present model.

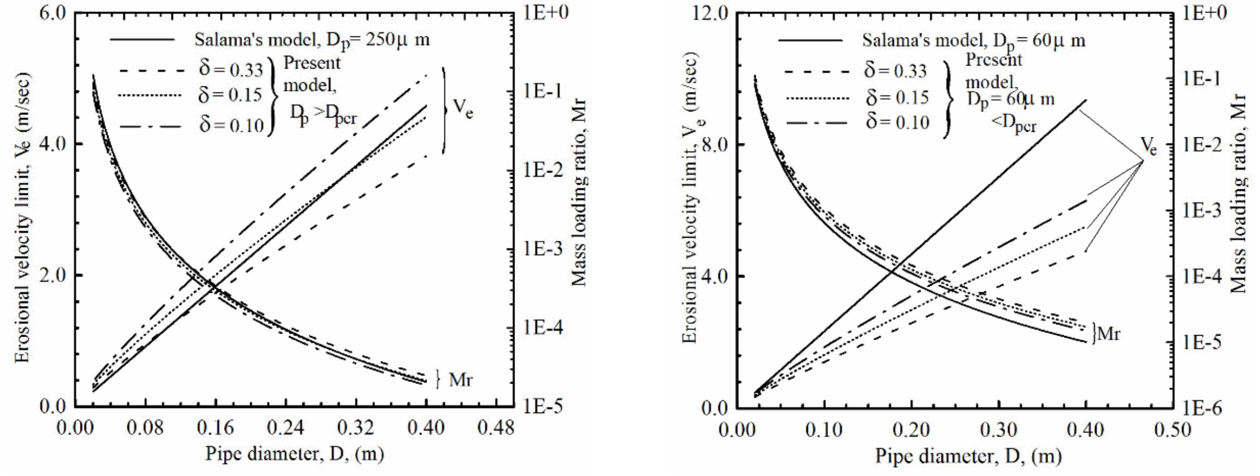

a- Large particle. b- Small particle.

Figure 11. Effect of pipe diameter on the erosional velocity limits, (allowable penetration rate = 0.1 mm/year, *BH* = 120, sharp particle and sand flow rate 5 kg/day).

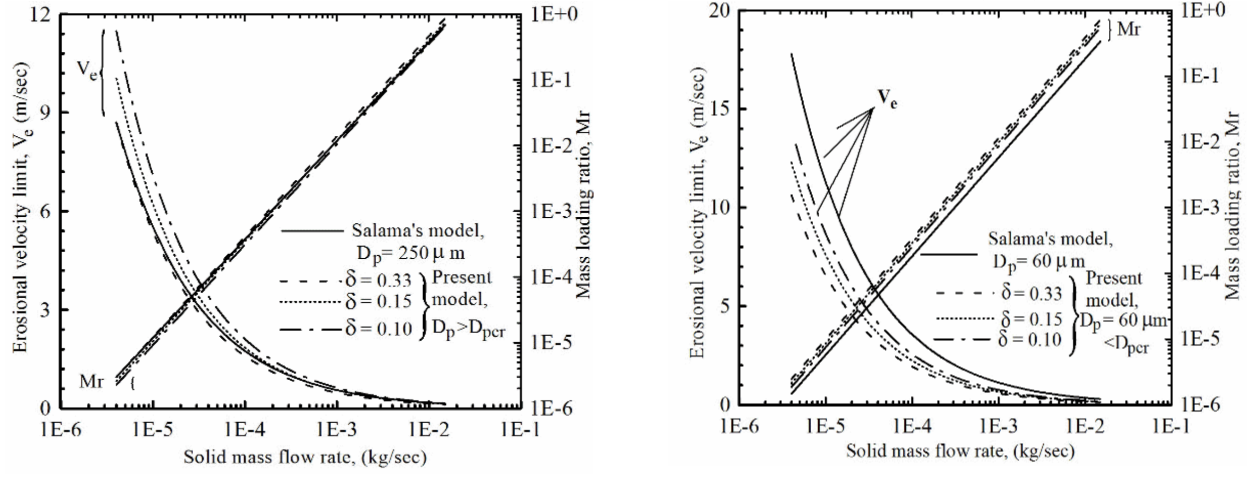

a- Large particle. b- Small particle.

Figure 12. Effect of solid mass flow rate on the erosional velocity limits, (allowable penetration rate = 0.1 mm/year, BH = 120, sharp particle and D = 0.2 m).

5. Conclusion

Erosion of bends conveying sand particles entrained in air flow was numerically simulated. Based on the obtained results, a new CFD based correlation was developed. The present results show an acceptable agreement with the available experimental data. It is concluded that the maximum allowable velocity should be decreased as the pipe diameter, particle size or mass loading ratio increase. The effect of fluid properties (density and viscosity), turbulent flow fluctuations and secondary flows may play important role in erosion prediction. These effects need to be further investigated.

Nomenclature

(Units are as stated here, unless noted otherwise in the text of the paper)

D	Diameter of bend, m
D_p	Particle diameter, μm
ER	Erosion rate, kg wall material/kg solid particles
Mr	Mass loading ratio, ($\overset{o}{m}_S / \overset{o}{m}_g$)

P_n	Penetration rate, µm/kg or µm/sec
R_C	Mean bend radius of curvature, m
Ro	Radius of bend outer wall, m
t	Time, sec
v	Mean radial velocity, m/s
V_e	Erosional velocity, m/s
v_p	Mean radial particle velocity, m/s
u	Mean axial gas velocity, m/s
U_o	Mean-bulk longitudinal velocity, m/sec
u_p	Mean axial particle velocity, m/s

Greek symbols

δ	Curvature ratio ($D/2R_C$)
θ	Axial coordinate along the bend, degree
ω_p	Particle angular velocity, rad/s

Appendix

TABLE 1. COMPARISONS BETWEEN THE PREDICTED PENETRATION RATES BY THE PRESENT SIMPLIFIED CORRELATION AND PUBLISHED DATA.

U_o m/sec	δ	Mr	Measured P_n, m/sec	Predicted maximum penetration rate, m/sec			
				Salama [4]	Wang and Shirazi [6]	McLaury et al. [7]	Present
Data based on Bourgoyne [3] (D_p = 350 µm, D = 0.0525 m, particles are semi-rounded, BH = 120 and 140, ρ_p = 2650 kg/m^3 and ρ_w = 7800 kg/m^3, prediction of Salama based on S_m = 33.							
32	0.333	0.554	3.74E-07	2.96E-07	1.06E-06	–	5.65E-07
47	0.333	0.553	3.32E-07	9.39E-07	–	–	1.55E-06
72	0.333	0.632	1.65E-06	3.84E-06	–	–	5.37E-06
93	0.333	0.541	3.70E-06	7.09E-06	–	–	9.14E-06
98	0.333	0.470	4.23E-06	7.22E-06	–	–	9.24E-06
98	0.333	0.547	4.94E-06	8.41E-06	–	–	10.6E-06
103	0.333	0.527	5.29E-06	9.39E-06	–	–	11.7E-06
122	0.333	0.502	3.43E-05	1.49E-05	4.29E-05	–	1.75E-05
167	0.333	0.471	3.73E-05	3.58E-05	–	–	3.76E-05
169	0.333	0.570	4.77E-05	4.48E-05	–	–	4.61E-05
177	0.333	0.760	8.33E-05	6.89E-05	1.01E-04	–	6.77E-05
177	0.333	0.634	7.38E-05	5.74E-05	8.40E-05	–	5.74E-05
178	0.333	0.624	6.52E-05	5.75E-05	–	–	5.74E-05
203	0.333	0.563	7.76E-05	7.69E-05	–	–	7.38E-05
205	0.333	0.716	7.96E-05	1.01E-04	–	–	9.43E-05
222	0.333	0.524	7.01E-05	9.33E-05	–	–	8.75E-05
108	0.333	0.178	3.56E-06	3.67E-06	6.85E-06	–	4.95E-06
109	0.333	0.326	5.64E-06	6.90E-06	–	–	8.78E-06
108	0.333	0.343	5.29E-06	7.04E-06	1.32E-05	–	8.96E-06
104	0.333	0.567	9.88E-06	1.04E-05	–	–	12.8E-06
108	0.333	0.610	1.38E-05	1.25E-05	2.34E-05	–	1.51E-05
108	0.333	0.740	1.37E-05	1.52E-05	2.84E-05	–	1.80E-05
107	0.333	0.107	1.43E-05	2.13E-05	–	–	3.03E-05
111	0.333	0.133	2.23E-05	2.97E-05	5.96E-05	–	4.08E-05
107	0.333	0.216	3.56E-05	4.33E-05	–	–	5.76E-05
106	0.333	0.233	3.26E-05	4.48E-05	–	–	5.95E-05
103	0.333	2.792	2.96E-05	4.98E-05	–	–	5.31E-05
100	0.333	0.143	3.91E-06	–	–	–	3.31E-06
100	0.333	0.296	5.31E-06	–	–	–	6.39E-06
100	0.333	0.529	9.84E-06	–	–	–	1.08E-05
100	0.333	0.596	1.23E-05	–	–	–	1.21E-05
100	0.333	0.722	1.23E-05	–	–	–	1.44E-05
100	0.333	1.057	1.30E-05	–	–	–	2.03E-05

100	0.333	1.374	1.84E-05	—	—	—	2.58E-05
100	0.333	2.187	3.08E-05	—	—	—	3.93E-05
100	0.333	2.329	2.88E-05	—	—	—	4.16E-05
100	0.333	2.735	2.78E-05	—	—	—	4.82E-05
116	0.190	1.160	5.74E-05	2.96E-05	—	6.02E-05	2.81E-05
141	0.174	0.517	3.32E-05	2.37E-05	3.44E-05	4.13E-05	1.99E-05
107	0.174	1.468	4.94E-05	2.93E-05	4.60E-05	5.51E-05	2.48E-05
141	0.174	0.474	3.02E-05	2.17E-05	3.15E-05	3.78E-05	1.83E-05
107	0.174	1.153	4.35E-05	2.31E-05	3.61E-05	4.33E-05	1.99E-05
111	0.154	1.911	6.15E-05	4.26E-05	6.45E-05	7.55E-05	3.29E-05
141	0.154	0.540	4.10E-05	2.47E-05	3.50E-05	4.09E-05	1.96E-05
141	0.154	0.221	1.53E-05	1.01E-05	1.44E-05	1.68E-05	0.87E-05
148	0.154	0.398	3.20E-05	2.11E-05	3.15E-05	3.45E-05	1.69E-05
111	0.111	1.396	2.12E-05	3.11E-05	—	4.63E-05	2.09E-05
Data based on Bourgoyne [29] (D_p = 350 μm, D = 0.1575 m, particle are semi-rounded, BH = 120, ρ_p = 2650 kg/ m^3 and ρ_w = 7800 kg/m^3.							
30.9	0.500	1.692	7.41E-07	—	—	—	19.9E-07
66.38	0.500	0.926	8.00E-06	—	—	—	9.44E-06
76.59	0.500	0.804	1.00E-05	—	—	—	1.21E-05
67.99	0.500	0.724	8.00E-06	—	—	—	8.04E-06
77.68	0.500	0.425	5.00E-06	—	—	—	7.04E-06
97.67	0.500	0.601	1.60E-05	—	—	—	1.76E-05
59.44	0.333	1.643	9.00E-06	—	—	—	1.11E-05
61.68	0.333	0.691	4.00E-06	—	—	—	5.57E-06
98.43	0.333	0.711	2.80E-05	—	—	—	1.95E-05
99.39	0.333	1.028	3.20E-05	—	—	—	2.80E-05
101.7	0.333	0.152	6.00E-06	—	—	—	5.26E-06
103.2	0.333	0.385	1.50E-05	—	—	—	1.27E-05
Data reported in [4, 6 and 7] (data of Tolle and Greenwood), D_p = 300 μm, D = 0.0525 m, particles are sharp, BH = 109, ρ_p = 2650 kg/ m^3 and ρ_w = 7800 kg/m^3, prediction of Salama based on S_m = 5.5.							
9.15	0.333	0.037	1.90E-09	3.37E-09	4.402E-09	2.36E-09	3.32E-09
12.2	0.333	0.028	2.82E-09	5.98E-09	6.182E-09	3.88E-09	5.94E-09
15.25	0.333	0.022	6.66E-09	9.30E-09	7.587E-09	5.71E-09	8.72E-09
18.3	0.333	0.019	8.11E-09	1.35E-08	9.647E-09	7.84E-09	11.9E-09
21.35	0.333	0.016	1.08E-08	1.83E-08	1.19E-08	1.03E-08	1.55E-08
24.4	0.333	0.014	1.44E-08	2.39E-08	1.433E-08	1.29E-08	1.96E-08
27.45	0.333	0.012	1.59E-08	3.03E-08	1.648E-08	1.59E-08	2.40E-08
30.5	0.333	0.011	1.81E-08	3.74E-08	1.873E-08	1.90E-08	2.88E-08
Data reported in [4 and 7] (data of Weiner and Tolle), D_p= 300 μm, D = 0.0525 m, particles are sharp, BH = 109, ρ_p = 2650 kg/ m^3 and ρ_w = 7800 kg/m^3, prediction of Salama based on S_m = 5.5.							
21.35	0.333	0.303	5.16E-09	2.43E-08	—	1.35E-08	15.6E-09
30.5	0.333	0.305	1.82E-08	4.90E-08	—	2.49E-08	3.91E-08
Data based on Bikbaev et al. [27], D_p = 295 μm, D = 0.05 m, particle are semi-rounded, BH = 120, ρ_p = 2580 kg/ m^3 and ρ_w = 7800 kg/m^3.							
54.8	0.066	0.570	2.31E-06	—	—	—	1.05E-06
54.8	0.066	1.390	2.87E-06	—	—	—	2.36E-06
54.8	0.066	2.100	3.74E-06	—	—	—	3.43E-06
54.8	0.066	2.330	4.26E-06	—	—	—	3.77E-06
33.1	0.195	4.350	1.94E-06	—	—	—	3.51E-06
39.2	0.195	3.010	2.92E-06	—	—	—	3.92E-06
50	0.195	2.930	5.03E-06	—	—	—	7.25E-06
54.8	0.195	2.100	5.97E-06	—	—	—	6.82E-06
Data based on Bikbaev et al. [28], D_p = 295 μm, D = 0.05 m, particle are semi-rounded, BH = 120 ρ_p = 2580 kg/ m^3 and ρ_w = 7800 kg/m^3.							
50	0.208	2.800	4.66E-06	—	—	—	4.78E-06
50	0.139	2.800	3.97E-06	—	—	—	6.04E-06
50	0.119	2.800	3.28E-06	—	—	—	5.56E-06
50	0.064	2.800	2.42E-06	—	—	—	3.41E-06

References

[1] TÜV NEL Limited, Erosion in elbows in hydrocarbon production systems: Review document, Research Report 115 for the Health and Safety Executive 2003.

[2] API, "API RP 14E Recommended practice for design and installation of offshore production platform piping systems", American Petroleum Institute, 5th Edition, Washington, DC, 1991.

[3] Bourgoyne, A.T., Experimental study of erosion in diverter systems due to sand production, Proc. SPE/ IADC Drilling Conf., New Orleans, Louisiana, Feb., 1989, pp 807-816.

[4] Salama, M. M., An alternative to API 14E erosional velocity limits for sand-laden fluids, Trans. of ASME, J. of Energy Resources Tech., Vol. 122, 2000, pp. 71-77.

[5] Shirazi, S.A., Shedley, J.R., McLaury, B.S. and Rybicki, E.F., A procedure to predict solid particle erosion in elbows and tees, Trans of ASME, J. of Pressure Vessel Tech., Vol. 117, 1995, pp. 45-52.

[6] Wang, J. And Shirazi, S.A., A CFD based correlation for erosion factor for long-radius elbows and bends, Trans. of ASME, J. of Energy Resources Tech., Vol. 125, 2003, pp. 26-34.

[7] McLaury, B.S., Shirazi, S.A., Shadley, J.R., and Rybicki, E.F., How operating and environmental conditions affect erosion, NACE Int. Annual Conf., Corrosion99, San Antonio, TX, USA, April 25-30, 1999, Paper No. 34.

[8] Huser, A. and Kvernvold, O., Prediction of sand erosion in process and pipe components, Proc. 1st North American Conf. on Multiphase Technology. Banff, Canada, 1998, pp. 217 – 227.

[9] Haugen, K., Kvernvold, O., Ronold, A. and Sandberg, R. Sand erosion of wear resistant materials: Erosion in choke valves Wear, Vol. 186-187, 1995, pp. 179-188.

[10] El-Behery, S.M., Hamed, M.H., El-kadi, M.A and Ibrahim, KA., CFD prediction of air-solid flow in 180° curved duct, Powder Technology, Vol. 191, 2009, pp. 130-142.

[11] Eghlimi, A., Kouzoubov, A., Fletcher, C.A.J., A new RNG-based two-equation model for predicting turbulent gas-particle flows, Proc. 1st Int. Conf. on CFD in Mineral & Metal Processing and Power Generation Industries, Melbourne, Australia, July 3-4, 1997.

[12] Launder, B.E. and Sharma B.I., Application of the energy-dissipation model of turbulence to the calculation of flow near a spinning disc, Letters in Heat and Mass Transfer, Vol. 1, 1974, pp. 131-138.

[13] Chen, Y.S. and Kim, S.W., Computation of turbulent flows using an extended k-ε turbulence clouser model, NASA CR-179204, 1987.

[14] Lun, C.K.K. and Liu, H.S., Numerical simulation of dilute turbulent gas-solid flows in horizontal channels, Int. J. Multiphase flow, Vol. 23, 1997, pp. 575-605.

[15] Kladas, D.D. and Deorgiou, D.P., A Relative Examination of CD–Re Relationships used in Particle Trajectory Calculations, Trans. of ASME, J. of Fluids Engineering, Vol. 115, 1993, pp. 162-165.

[16] Saffman, P.G., The lift on a small sphere in a slow shear flow, J. Fluid Mech., Vol. 22, Part 2, 1965, pp. 385-400.

[17] Mei, R., An approximate expression for the shear lift force on a spherical particle at finite Reynolds number, Int. J. Multiphase Flow, Vol. 18, 1992, pp. 145-147.

[18] Crowe, C., Sommerfeld, M. and Tsuji, Y., Multiphase flow with droplets and particles, CRC Press, Florida, USA, 1998.

[19] McLaury, B.S., Predicting solid particle erosion resulting from turbulent fluctuation in oilfield geometries, PhD Dissertation, The University of Tulsa, Tulsa, Oklahoma, USA, 1996.

[20] Ng, E.Y.K. and Tan, S.T., Comparison of various turbulence models in rotating machinery blade-to-blade passages, Int. J. of Rotating Machinery, Vol. 6, 2000, pp. 375-382.

[21] Heinl, E. and Bohent, M., Calculation of particle-wall adhesion in horizontal gas-solid flow using CFD, Powder Tech., Vol. 159, 2005, pp. 95-104.

[22] Sommerfeld, M. and Huber, N., Experimental analysis and modeling of particle-wall collisions, Int. J. Multiphase Flow, Vol. 25, 1999, pp. 1457-1489.

[23] Patankar, S.V., Numerical heat transfer and fluid flow, McGraw-Hill, New York, USA, 1983.

[24] Yilmaz, A. and Levy, E.K., Formation and dispersion of ropes in pneumatic conveying, Powder Tech., Vol. 114, 2001, pp. 168-185.

[25] Kliafas, Y. and Holt, M., LDV measurements of a turbulent air-solid two-phase flow in a 90o bend", Experiments in Fluids, Vol. 5, 1987, pp. 73-85.

[26] Wadke, P.M., Pitt, M.J., Kharaz, A., Houslow, M.J. and Salman, A.D., Particle trajectory in a pipe bend, Advanced Powder Tech., Vol. 16, 2005, pp. 659-675.

[27] Bikbiaev, K.A., Krasnov, V.I., Maksimenko, M.I., Berezin, V., Zhilinskii, I.B., and Otroshko, N.T., Main factors affecting gas abrasive wear of elbows in pneumatic conveying pipes, Chemical Petroleum Eng., Vol. 9, 1973, pp. 73-75.

[28] Bikbiaev, F.A., Maksimenko, M.I., Berezin, V.L., Krasnov, V.L., and Zhilinskii, I.B., Wear on branches in pneumatic conveying ducting, Chemical Petroleum Eng., Vol. 8, 1972, pp. 465-466.

[29] Bourgoyne, A.T., Casariego, V. and Kelly, O.A., Integrity of diverter systems under abrasive, multi-phase flow, Summary Report, Petroleum Eng. Department, Louisiana State University, Baton Rouge, Louisiana, 1991.